SCIENTIFIC REPORTS

OPEN

SUBJECT AREAS:

NANOPARTICLES

MAGNETIC PROPERTIES AND MATERIALS

Received
19 November 2014

Accepted
12 March 2015

Published
15 April 2015

Correspondence and requests for materials should be addressed to K.N.T. (k.trohidou@inn.demokritos.gr)

Enhanced Magnetic Properties in Antiferromagnetic-Core/Ferrimagnetic-Shell Nanoparticles

Marianna Vasilakaki[1], Kalliopi N. Trohidou[1] & Josep Nogués[2,3]

[1]Institute of Nanoscience and Nanotechnology, NCSR ''Demokritos'', Aghia Paraskevi, Attiki, 15310, Greece, [2]ICN2 - Institut Catala de Nanociencia i Nanotecnologia, Campus UAB, 08193 Bellaterra (Barcelona), Spain, [3]ICREA - Institució Catalana de Recerca i Estudis Avançats, Barcelona, Spain.

Bi-magnetic core/shell nanoparticles are gaining increasing interest due to their foreseen applications. Inverse antiferromagnetic(AFM)/ferrimagnetic(FiM) core/shell nanoparticles are particularly appealing since they may overcome some of the limitations of conventional FiM/AFM systems. However, virtually no simulations exist on this type of morphology. Here we present systematic Metropolis Monte Carlo simulations of the exchange bias properties of such nanoparticles. The coercivity, H_C, and loop shift, H_{ex}, present a non-monotonic dependence with the core diameter and the shell thickness, in excellent agreement with the available experimental data. Additionally, we demonstrate novel unconventional behavior in FiM/AFM particles. Namely, while H_C and H_{ex} decrease upon increasing FiM thickness for small AFM cores (as expected), they show the opposite trend for large cores. This presents a counterintuitive FiM size dependence for large AFM cores that is attributed to the competition between core and shell contributions, which expands over a wider range of core diameters leading to non-vanishing H_{ex} even for very large cores. Moreover, the results also hint different possible ways to enhance the experimental performance of inverse core/shell nanoparticles for diverse applications.

In recent years, the development of novel synthetic routes, allowing the delicate control of the morphology of nanoparticles, has triggered the interest in more complex magnetic structures such as bi-magnetic core/shell nanoparticles[1]. Among them, ferromagnetic (FM)/antiferromagnetic (AFM) systems are the most studied due to their exchange bias properties (e.g., loops shifts or coercivity enhancement)[2]. These systems not only combine the properties of the different constituents, but the core/shell interactions can provide an additional degree of freedom to improve the properties, thus opening new avenues for innovative applications of magnetic nanoparticles, ranging from energy storage[3–8] to biomedicine[9–11]. Interestingly, currently, there is an increasing interest in, so-called, inverted structures (see Fig. 1), where the shell is FM or ferrimagnetic (FiM) and the core is AFM, containing for example Mn oxides[12–18], Fe oxides[19–29], Co oxides[30–36], Cr oxides[37–39], metallic FePt[40] or even multiferroic $BiFeO_3$ (Refs. 41,42). This type of inverted structures overcomes some of the limitations of conventional systems, since the AFM structure (and thus its magnetic properties) can be much better controlled in the core than in the shell (where usually it is forced to grow in non-ideal conditions). It has been demonstrated, experimentally and theoretically, that the poor crystallinity of the AFM counterpart can result in considerably inferior exchange bias properties[43,44]. In fact, inverted structures have already demonstrated very large coercivities and loop shifts, tunable blocking temperatures, enhanced Néel temperatures or proximity effects[12–42] and have been proposed as potential magnetoelectric random access memories[41]. However, despite their potential, systematic studies of size effects (i.e., core diameter or shell thickness) are still rather scarce[12,16,22,25,33–35]. Remarkably, similar effects of the role of the position of the different magnetic phases (core vs shell) also arise in other types of bi-magnetic core/shell nanoparticles such as hard-FM/soft-FM vs. soft-FM/hard-FM nanoparticles, where systems with the hard counterpart in the core can have enhanced or different properties with respect to the ones with soft-FM cores[45,46]. Thus, understanding the role of the position of the diverse magnetic phases (core vs. shell) is of chief importance in the development of novel applications of bi-magnetic core/shell nanoparticles.

From the magnetic point of view, one can identify two main types of inverted structures depending on the transition temperature of the materials. Thus, "single inverted" systems are those where the Curie temperature of the FM, T_C, is larger than the Néel temperature of the AFM, T_N, i.e., $T_C > T_N$, e.g., FeO/Fe_3O_4. On the other hand, if $T_N > T_C$, the systems are usually denoted "doubly inverted", e.g., MnO/Mn_3O_4. Although this type of structure

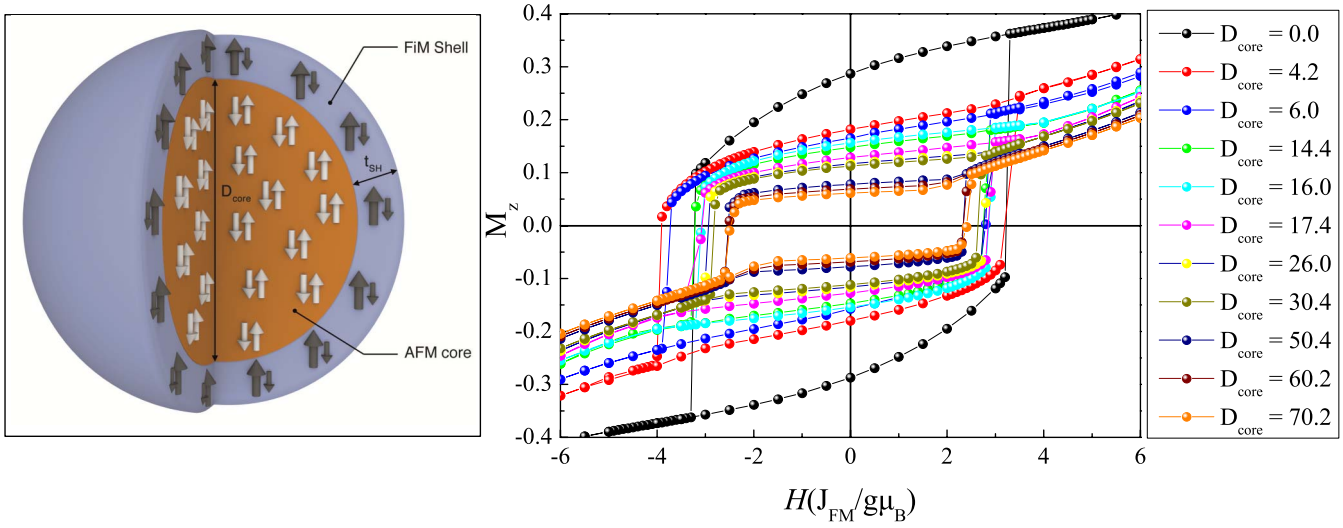

Figure 1 | Schematic representation and core size dependence of the hysteresis loops. (left) Schematic representation of the inverse AFM/FiM core/shell structure and (right) hysteresis loops of the doubly inverted nanoparticles, for different AFM core sizes (D_{core}) and constant FiM shell thickness of four lattice spacings.

is seldom studied in thin film systems, the available results evidence rather interesting properties[47,48]. Similarly, doubly inverted core/shell nanoparticles exhibit some novel properties such as a non-monotonic dependence of the coercivity and the loop shift on the core size[12].

From the numerical simulation point of view, the mechanisms and the factors that influence the exchange bias behavior in conventional core/shell nanoparticles, i.e., soft FM core/hard AFM[49,50] or FiM shell nanoparticles[46,51,52] have been fairly investigated[53,54]. These studies support that the exchange bias field depends mainly on the structure of the interface (uncompensated spins) and the coercive field on the particle size. Studies of inverted, AFM/FM, structures (hard AFM/soft FM) are far scarcer[55,56] and, in fact, there are no reports on doubly inverted structures. Notably, the factors responsible for the observed enhanced magnetic behavior of the inverse structure are largely unknown.

Herein, we investigate the core and shell size dependence of the magnetic properties of hard FiM nanoparticles in doubly inverted ($T_N > T_C$) AFM/FiM core/shell structures using Monte Carlo (MC) simulations. We consider a broad range of core sizes and shell thicknesses to elucidate the optimum conditions for improved properties for diverse possible applications. The results clearly replicate the non-monotonic dependence of the exchange bias properties observed experimentally. Namely, for very small core sizes both coercive (H_C) and exchange bias (H_{ex}) sharply increase as the core size becomes larger. However above a certain size H_C and H_{ex} start to decrease, thus exhibiting a maximum. Further, they show that the dependence of the magnetic properties on the FiM thickness depends critically on the size of the AFM core, leading to H_C and H_{ex} proportional to the FiM thickness for large AFM cores. The origin of these unusual effects is shown to arise from the competition between the AFM core spins and the hard FiM shell.

Results

Shown in the right panel of Fig. 1 are the hysteresis loops for doubly inverted nanoparticles for various core diameters, D_{core}, and a constant shell thickness, t_{SH} of four lattice spacings, $t_{SH} = 4$. The saturation magnetization of the loops decreases for larger D_{core} as expected from the zero net magnetic moment of the AFM core. Moreover, it can be seen that the loops exhibit both H_C and H_{ex}, which have different behavior for the diverse D_{core}. The dependence of H_C and H_{ex} on D_{core} for $t_{SH} = 4, 6, 8$ is shown in Fig. 2.

The results clearly show that inverted structures can result in sizable loop shifts and coercivity enhancements, similar to conventional FM/AFM structures[2]. Nevertheless, contrary to conventional systems, a strong non-monotonic behavior is observed. Interestingly, both H_C and H_{ex} exhibit maximum values for rather small D_{core}. Moreover, the maximum H_C is obtained for very small D_{core} (e.g., $D_{core} = 4.2$ for $t_{SH} = 4$) whereas the maximum H_{ex} is observed for slightly larger D_{core} (e.g., $D_{core} = 6$ for $t_{SH} = 4$). These results are in qualitative agreement with the experimental doubly inverse MnO/Mn_3O_4 nanoparticles case, which also shows an analogous non-monotonic dependence of H_C and H_{ex} on D_{core} (Ref. 12).

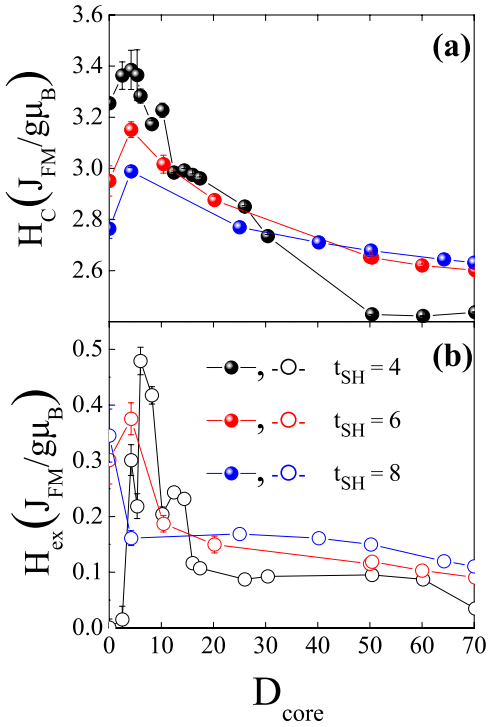

Figure 2 | Core size dependence of the coercivity and the exchange bias. Dependence of the coercivity, H_C (a) and exchange bias shift, H_{ex} (b) on the AFM core size, D_{core} for the doubly inverted ($T_C < T_N - J_{core} > J_{shell}$) structures for $t_{SH} = 4$, 6 and 8.

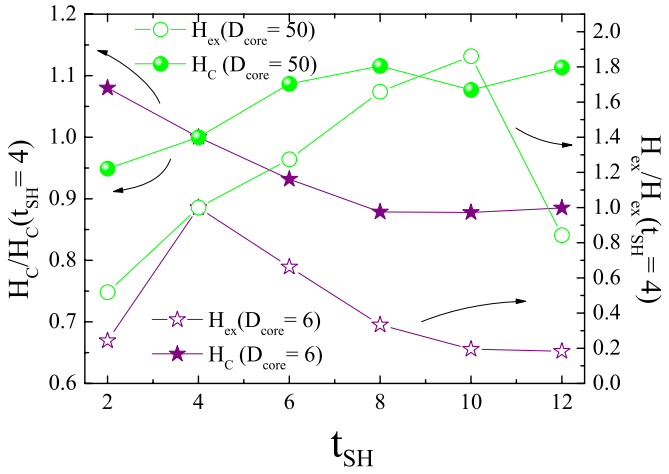

Figure 3 | Shell size dependence of the coercivity and the exchange bias. Dependence of the normalized H_C and H_{ex} on t_{SH} for $D_{core} = 6$ and 50.

Remarkably, both H_C and H_{ex} decrease considerably slow with increasing D_{core}. In fact, H_C and H_{ex} stabilize for large D_{core} values and H_{ex} does not vanish even for $D_{core} = 70$. The overall behavior of both H_C and H_{ex} is similar for the three t_{SH}. Explicitly, they all exhibit non-monotonic behavior with maxima both in H_C and H_{ex} at small D_{core} values. However, a more careful analysis of the data reveals several appealing features. Concerning H_C, it decreases slower as D_{core} increases for thicker t_{SH}, leading to a crossover behavior for large D_{core}. Interestingly, although for small D_{core} H_C decreases for thicker t_{SH}, the coercivity enhancement, i.e., $\Delta H_C/H_C$, becomes larger for thicker shells, reaching almost 10% for $t_{SH} = 8$. Regarding H_{ex}, two remarkable features are worth mentioning. First, the maximum H_{ex} is obtained for smaller D_{core} as t_{SH} increases. Secondly, similar to H_C, H_{ex} also exhibits a cross over behavior. As expected from the inverse FM thickness dependence of exchange bias observed in thin films or conventional core/shell particle[2], for small D_{core} H_{ex} decreases for larger t_{SH}. However, this trend is reversed for large D_{core} and, counterintuitively, H_{ex} increases for larger t_{SH}. This is summarized in Fig. 3, where it can be clearly seen that while for small core sizes H_C and H_{ex} exhibit the conventional inversely proportional to t_{SH} behavior (i.e., $\sim \propto 1/t_{SH}$), for large cores the behavior is against what is expected for an interface effect and is proportional to t_{SH} (i.e., $\sim \propto t_{SH}$). This trend is somewhat broken for H_{ex} for exceedingly small t_{SH} in the case of small D_{core} and for large t_{SH} in the case of large D_{core}.

The simulations have revealed a number of notable results which, in some cases, are in clear contrast with conventional exchange bias wisdom in thin film and conventional FM/AFM core/shell nanoparticles: (i) both H_C and H_{ex} exhibit a strong non-monotonic behavior with D_{core}; (ii) the maximum H_C and H_{ex} is obtained for rather small D_{core}, with sizes comparable to those of the shell; (iii) the largest H_C is obtained for smaller D_{core} than for H_{ex}; (iv) although H_{ex} and H_C increase for thinner t_{SH} for small D_{core}, they show an opposite behavior at large D_{core}.

Discussion

To unveil the origin of these novel effects, the number of total and uncompensated spins in the core, interface, shell and surface have been evaluated. Note that uncompensated spins are those spins that due to their local environment of reduced number of neighbors feel a smaller mean field and can thus act more independently. As can be seen in the Fig. 4, the relative number of spins in the different positions with respect to the total number of spins depends strongly on the D_{core} and t_{SH} dimensions. Plotted in Fig. 5 is the absolute number of uncompensated spins N_{up}-N_{dw} as a function of the core size, for $t_{SH} = 4$, normalized to the total number of spins, N_{tot}, for the core interface (IF), the shell IF and the surface, taking into account the fact that at the surface and the shell IF the spin magnitude is 1 and 1.5 respectively in the two sublattices. Hence, for the core IF region the normalized number of uncompensated spins is $Abs[(N_{AFMup}-N_{AFMdw})/(N_{AFMup} + N_{AFMdw} + N_{FiMup} + N_{FiMdw}*1.5)]$ while in the other regions is $Abs[(N_{FiMup}-N_{FiMdw}*1.5)/(N_{AFMup} + N_{AFMdw} + N_{FiMup} + N_{FiMdw}*1.5)]$. Notably, the notation up and down spins, introduced firstly by Néel[57], is just schematic to indicate the spins in the two sublattices. Consequently, in the simulations, where the anisotropy parameters are not particularly strong anywhere in the nanoparticle, these spins do not actually act collinearly. Moreover, it should be emphasized that the number of spins and uncompensated spins is solely governed by geometry. Thus, it is important to emphasize that observed fluctuations in the number of uncompensated spins, especially for small core sizes are due to geometrical effects.

For very small core sizes, in the range between 2.5–5.35 lattice spacings, the number of uncompensated spins at the core IF and shell IF is very small, while the number of uncompensated spins at the surface of the shell is considerably larger (Fig. 5). Thus, for very small D_{core} H_{ex} is dominated by the uncompensated spins from the surface of the FiM shell. Although the number of surface spins is relatively small their radial character keeps them pinned on the surface, resulting in finite exchange bias. As D_{core} increases, in the range between 5.35 and 12.4 lattice spacings, the number of uncompensated spins in both the core IF and the shell IF increases (Fig. 5). The maximum of the H_{ex} corresponds to the core size that gives the maximum value of the number of uncompensated spins at the shell interface and a sizable contribution of the core IF and surface uncompensated spins. Thus, the shell IF and the surface mainly contribute to the maximum H_{ex}. As D_{core} becomes even larger, for core sizes in the range 12.4–25 lattice spacings, the number of uncompensated spins of the core IF becomes almost negligible and finally vanishes for $D_{core} > 25$ lattice spacings, while the average number of uncompensated spins at the shell IF and the surface slowly decreases, leveling off for very large D_{core}. This behavior is similar to one observed for H_{ex} (Fig. 2). Consequently, for large D_{core} H_{ex} is controlled mainly by the shell. Thus, the evolution of the uncompensated spins can qualitatively explain the overall dependence of H_{ex} on D_{core}. Interestingly, the large exchange J_{core} of the doubly inverted structure results in an extra anisotropy in the core spins. This gives rise to a stronger resistance of the core spins to be dragged by the reversal of the shell spins, leading to a non-vanishing H_{ex} even for large D_{core} (in the range 30–60.2 lattice spacings). For this D_{core} range, although the number of core spins dominates, the shell spins still contribute to the exchange bias properties, acting as a pining center and therefore competing with the core spins over a wide range of core sizes, where the shell still has a sizeable contribution.

These arguments can also account for the non-monotonic behavior of $H_{ex}(t_{SH})$ for the different D_{cores} observed in Fig. 3. Namely, in the case of small D_{core} as t_{SH} becomes exceedingly small (e.g. $t_{SH} = 2$) the number of surface spins and shell interface spins (see Fig. 4) dominate over core spins, leading to a H_{ex} reduction. On the other hand for large D_{cores}, as t_{SH} becomes sufficiently large the competition between core spins and shell spins increases resulting in an increase of H_{ex}.

Concerning H_C, for very small core sizes we have contribution mainly from the shell and the maximum occurs for the core size where the total number of spins from the shell plays the dominant role (see inset in Fig. 5). For larger core sizes, the extra anisotropy induced by the shell acting as pinning center (as N_{core} starts to increase) results in a slow decrease H_C as D_{core} is increased.

Regarding the role of the shell thickness, given the larger shells in the $t_{SH} = 6$ and 8 (compared to $t_{SH} = 4$) the competition between the core and shell contributions (i.e., when then number of core spins become larger than the number of shell spins; see Fig. 4) occurs at

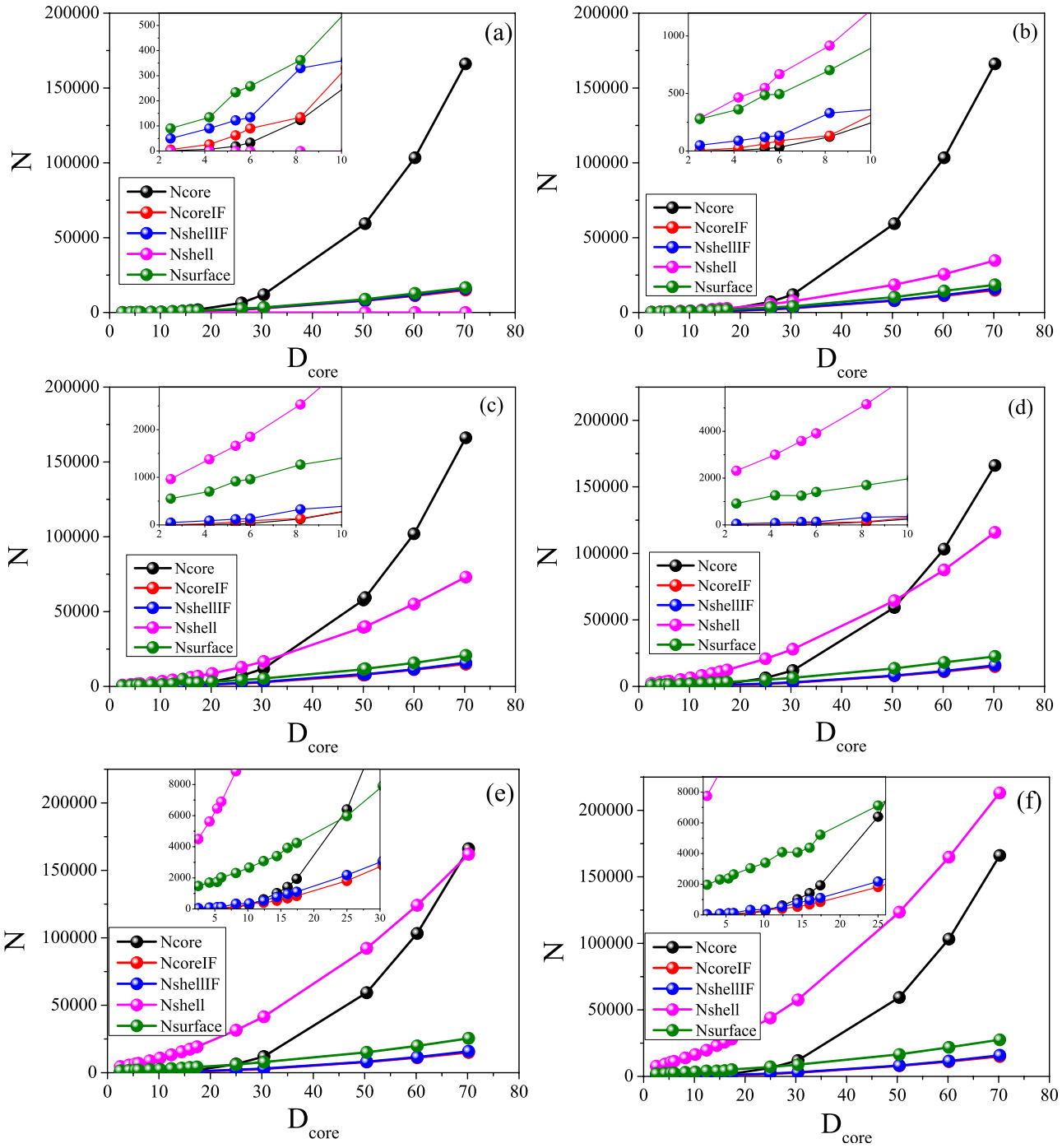

Figure 4 | Size dependence of the total number of spins. Number of spins (N) in each region for various core diameters and shell thickness 2 (a), 4 (b), 6(c), 8(d), 10(e) and 12(f) lattice spacings. Shown in the insets are enlarged views of N vs. D_{core} for low D_{core}.

different D_{core}. The boundaries are roughly $D_{core} \sim 25$, 30 and 50 for $t_{SH} = 4$, 6 and 8, respectively. Consequently, the decrease of H_{ex} and H_C for large D_{core} is pushed to larger D_{core} as t_{SH} increases. This gives rise to the crossover from the conventional FM thickness dependence of exchange bias systems (i.e., $t_{FM} \uparrow \rightarrow H_{ex}$, $H_C \downarrow$) at small D_{core} to the counterintuitive reversed behavior ($t_{FM} \uparrow \rightarrow H_{ex}$, $H_C \uparrow$) for large D_{core}.

Notably, this unusual behavior is to some extent different in single inverted AFM core/FiM shell nanoparticles shown in Fig. 6 (i.e., $T_N < T_C - J_{core} < J_{shell}$). Namely, while H_C exhibits a $H_C \propto t_{SH}$ dependence for large D_{cores} similar to the doubly inverted case, H_{ex} shows this inverse behavior only in a very narrow range of D_{cores} since H_{ex} vanishes at large D_{cores}. In this case since J_{core} is weaker there is no competition between the core and the shell. Thus, the shell drags the core spins with the consequent decrease of H_{ex} and H_C. Consequently, the doubly inverted structures present improved properties compared to the single inverted ones, especially for large D_{cores}.

From the applications point of view some of the features unveiled from the simulations are rather attractive. One possible use of these structures could be to utilize the coercivity enhancement for small D_{core} to improve the performance of permanent magnets[58]. Given the higher H_C for thin shells, probably thin shells with small cores would be ideal for this type of purposes. Note that despite the loss of saturation magnetization, M_S (due to the zero M_S of the AFM core), since the core is so small the energy product (i.e., the figure of merit of

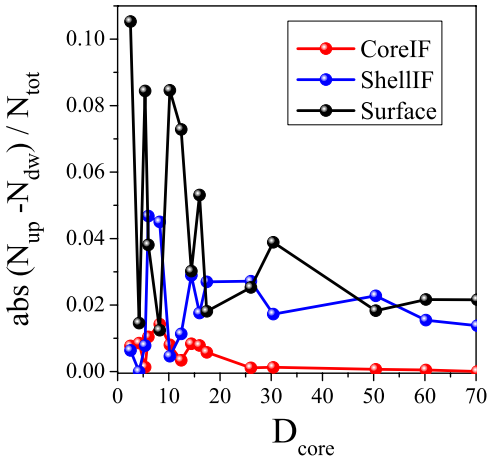

Figure 5 | Core size dependence of the number of uncompensated spins. Absolute number of uncompensated spins of the core IF, shell IF and surface normalized to the total number of spins, as a function of the core diameter, D_{core} (for $t_{SH} = 4$).

a permanent magnet) may actually be improved (similar to what has been observed in AFM/FM composites[59]) in these structures. For recording applications[3,4], where, for example, enhancement of the blocking temperature of very small nanoparticles may be pursued, perhaps larger coercivity enhancement, ΔH_C (which implies an increased effective anisotropy) may be more appealing. Thus, thicker shells with small cores would be more appropriate. Note that for this type of applications inverse AFM/FM structures may be more suitable than conventional FM/AFM, since the stray field of the nanoparticles (required for easy detection) would be less attenuated. For applications based on H_C, doubly inverted structures may be more attractive, especially if large cores are needed. Concerning applications requiring exchange bias, e.g., miniaturized magnetotransport

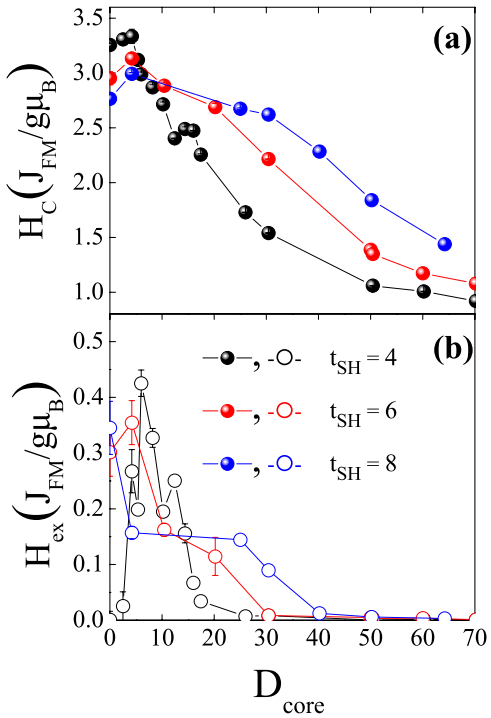

Figure 6 | Core size dependence of the coercivity and the exchange bias. Dependence of the coercivity, H_C (a) and exchange bias shift, H_{ex} (b) on the AFM core size, D_{core} for the single inverted ($T_C > T_N - J_{core} < J_{shell}$) structures for $t_{SH} = 4$, 6 and 8.

devices[6,41], the optimum D_{core}/t_{SH} configuration would depend on the exact H_C/H_{ex} required. For example, for large H_C and H_{ex}, then small t_{SH} with moderate D_{core} may be best. Nevertheless for cases where moderate H_C and H_{ex} are needed, large t_{SH} and D_{core} would be better.

Conclusion

In conclusion, the behavior of the exchange bias and the coercive field in doubly inverted AFM core/hard FiM shell nanoparticle systems have been shown to depend on the core size in a different way at various core size ranges. For very small core sizes there is contribution on H_{ex} from the surface uncompensated spins. For moderate core sizes the uncompensated spins of the core and the shell interface also contribute to the exchange bias, resulting in a maximum H_{ex} value. For even larger core diameters the exchange in the core, J_{core} and the AFM character of the core determine H_{ex}. For large D_{core} the whole shell plays the role of the shell IF, thus the exchange bias effect for these core sizes increases with shell thickness, in contrast to conventional systems. The study of the role of the shell thickness indicates that a sizable shell contribution is needed to ensure enhancement of the exchange bias properties. The improved magnetic properties can satisfy a range of technological demands.

Methods

For the study of the magnetic behavior of the nanoparticles we use the Monte Carlo simulation technique and the Metropolis algorithm[53]. We consider spherical nanoparticles of diameter D, expressed in lattice spacings, on a simple cubic lattice with inverted structure, consisting of an AFM core and a FiM shell (see Fig. 1-left panel). We take into account explicitly the microstructure of the system in an atomic scale. The spins of the nanoparticles are located at each lattice site of the core, the interface, the shell and the surface. They interact with nearest neighbours through Heisenberg exchange interactions and at each crystal site they experience a uniaxial anisotropy. At the surface of the particles, the crystal symmetry is reduced and consequently the anisotropy is stronger than in the bulk[60,61]. The FiM shell is considered as a layer surrounding the core.

In the presence of an external magnetic field, the total energy of the system is

$$E = -J_{core}\sum_{i,j\in core}\vec{s_i}\cdot\vec{s_j} - J_{shell}\sum_{i,j\in shell}\vec{s_i}\cdot\vec{s_j} - J_{IF}\sum_{i\in core, j\in shell}\vec{s_i}\cdot\vec{s_j} - K_{icore}\sum_{i\in core}(\vec{s_l}\cdot\hat{e_l})^2 - K_{ishell}\sum_{i\in shell}(\vec{s_l}\cdot\hat{e_l})^2 - \vec{H}\sum_{i}^{N}\vec{s_l} \quad (1)$$

Here $\vec{s_l}$ is the atomic spin at site i and $\hat{e_i}$ is the unit vector in the direction of the easy axis at site i. We consider the magnitude of the atomic spins in the two AFM sublattices equal to 1 and in the two FiM sublattices of the shell to be equal to 1 and 1.5, respectively. The first term in Eq. 1 gives the exchange interaction between the spins in the AFM core, while the second term gives the exchange interaction between the spins in the FiM shell. We consider two different cases, (i) single inverted with $T_C(shell) > T_N(core)$ and (ii) doubly inverted with $T_N(core) > T_C(shell)$. To take into account the difference in transition temperatures, for the first case we consider the exchange coupling constant of the core as $J_{core} = -0.5\ J_{FM}$ and that of the shell as $J_{shell} = -1.5\ J_{FM}$ where J_{FM} is the exchange coupling constant of a pure ferromagnet $J_{FM} = 1$ as reference value. In the doubly inverted structures, J_{shell} is maintained the same, but J_{core} in increased to account for the larger T_N. Thus, the exchange coupling constants are set to $J_{core} = -3.0\ J_{FM}$ and $J_{shell} = -1.5\ J_{FM}$. The third term gives the exchange interaction at the interface between the core and the shell. The interface includes the last layer of the AFM core and the first layer of the FiM shell. The exchange coupling constant of the interface J_{IF} is taken equal to that of the shell J_{SH}. The forth term gives the anisotropy energy of the AFM core, K_C. If the site i lies in the outer layer of the AFM core $K_{icore} = K_{IF}$ and $K_{icore} = K_C$ elsewhere (with $K_C = 0.05\ J_{FM}$ -i.e., a soft AFM- and $K_{IF} = 0.5\ J_{FM}$). The fifth term gives the anisotropy energy of the FiM shell, which is taken as $K_{SH} = 0.5\ J_{FM}$. If i lies in the outer layer (i.e., the surface) of the shell then the anisotropy is taken as $K_S = 1.4\ J_{FM}$, which is assumed to be radial (rather than uniaxial). The last term in Eq. 1 is the Zeeman energy.

The aim of our model is to qualitatively reproduce the magnetic behavior of this new class of advanced nanomaterials, therefore the parameters used in the simulations for the exchange and the anisotropy constants were chosen from a careful analysis of the experimental magnetic behavior of the nanoparticle system MnO (AFM)/Mn_3O_4 (FiM) (i.e., the most studied doubly-inverse system)[12]. Note that since ab initio electronic calculations cannot be performed for this type of complex nanoparticles the parameters were estimated by modifying the bulk values Mn_3O_4 and MnO taking into account the lower crystal symmetry at the interface and at the surface, which results in higher effective anisotropy energy in these regions. Nevertheless, the K parameters are weighted by their corresponding volume[49]. The exchange coupling parameters for the core, the interface, the shell and the surface are

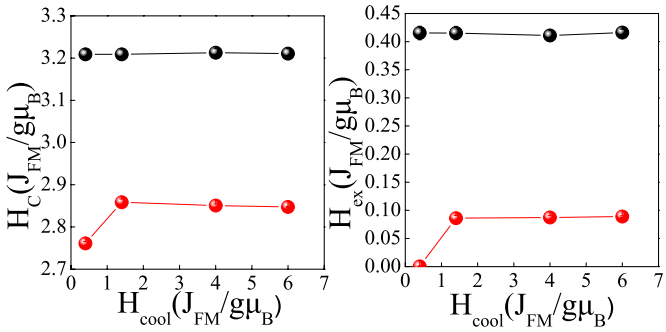

Figure 7 | Effect of the cooling field. Dependence of coercivity, H_C (left) and exchange bias, H_{ex} (right) on the cooling field, H_{cool}, for D_{core} = 8.2 (squares) and 26 (circles), with t_{SH} = 4.

considered here to be the same for all the different core and shell sizes since the exchange coupling parameters are short ranged and hence the influence of the second or third neighbors is almost negligible[62]. Moreover, it is worth noting that experimental studies of the detailed chemical characterization of MnO/Mn_3O_4 core/shell nanoparticles indicate that the interface between MnO and Mn_3O_4 is rather sharp[63], thus justifying our model.

Importantly, the chosen parameters roughly maintain the main experimental characteristics (i.e., $T_C(Mn_3O_4)/T_N(MnO) \sim 1/3$ and $K_{FiM}(Mn_3O_4)/K_{AFM}(MnO) \sim 50$) with simulated values of $T_C(Mn_3O_4)/T_N(MnO) \sim 1/3$ and $K_{FiM}(Mn_3O_4)/K_{AFM}(MnO) \sim 10$. Note that the smaller than bulk ratio $K_{FiM}(Mn_3O_4)/K_{AFM}(MnO)$ used in the simulations was chosen to take into account the possible worsening of the magnetic properties of the shell material due to structural deterioration of shell. Note, for example, that although the Mn_3O_4 shell in MnO/Mn_3O_4 core/shell nanoparticles exhibits a T_C close to bulk values, their H_C is usually smaller (i.e., lower $K(Mn_3O_4)$)[12,16–18].

We perform our simulations of the hysteresis loops on isolated nanoparticles using the Monte Carlo (MC) simulation technique with the implementation of the Metropolis algorithm[64]. The hysteresis loops are calculated after a field cooling procedure starting at temperature $T = 7.0\ J_{FM}/k_B$ down to $T_f = 0.01\ J_{FM}/k_B$, at a constant rate under a static magnetic field $H_{cool} = 4.0\ J_{FM}/g\mu_B$ directed along the z-axis. The value of H_{cool} was selected as the optimum value to observe maximum H_{ex} and H_C as Fig. 7 shows. The hysteresis loop shift on the field axis gives the exchange field $H_{ex} = -(H_{right}+H_{left})/2$. The coercive field is defined as $H_C = (H_{right}- H_{left})/2$. H_{right} and H_{left} are the points where the loop intersects the field axis. The coercive H_C and exchange H_{ex} fields are given in dimensionless $J_{FM}/g\mu_B$ units and the temperature T in J_{FM}/k_B.

In the Monte Carlo method, at each Monte Carlo step we select, at random, an atomic spin from the N spins of the nanoparticle and we make a small change in its orientation. This attempted change is accepted if it leads to the lowering of the system's energy or with a certain probability that corresponds to the Boltzmann probability. The process is repeated until equilibrium is reached. We have used 10^4 MC steps per spin (MCSS) at each field step and the results were averaged over 50–200 different samples (namely random numbers) depending on the size of the nanoparticle and the fluctuations in the values of the calculated fields. The standard deviation of the averages is depicted in the plots as error bars.

1. López-Ortega, A., Estarder, M., Salazar-Alvarez, G., Roca, A. G., & Nogués, J. Applications of exchange coupled bi-magnetic hard/soft and soft/hard magnetic core/shell nanoparticles. *Phys. Rep.* **553**, 1–32 (2015).
2. Nogués, J. *et al.* Exchange bias in nanostructures. *Phys. Rep.* **422**, 65–117 (2005).
3. Skumryev, V. *et al.* Beating the superparamagnetic limit with exchange bias. *Nature* **423**, 850–853 (2003).
4. Mishra, D. K., inventor; University of Louisiana at Lafayette, assignee. FeRh-FePt core shell nanostructure for ultra-high density storage media. United States patent 7, 964, 013. 2011 June 21.
5. Liu, X. S., Gu, B. X., Zhong, W., Jiang, H. Y. & Du, Y. W. Ferromagnetic/antiferromagnetic exchange coupling in $SrFe_{12}O_{19}$/CoO composites. *Appl. Phys. A* **77**, 673–676 (2003).
6. Groza, I., Morel, R., Brenac, A., Beigne, C. & Notin, L. Electrical and magnetic properties of Co/CoO core-shell clusters. *IEEE Trans. Magn.* **47**, 3355–3357 (2011).
7. Rostamnejadi, A. *et al.* Conventional and inverse magnetocaloric effects in $La_{0.45}Sr_{0.55}MnO_3$ nanoparticles. *J. Appl. Phys.* **110**, 043905 (2011).
8. Barbic, M. & Scherer, A. Magnetic nanostructures as amplifiers of transverse fields in magnetic resonance. *Sol. State Nucl. Magn. Res.* **28**, 91–105 (2005).
9. Rida, A., inventor; Spinomix, S. A., assignee. Tailored magnetic particles comprising a non-magnetic component and a magnetic core-shell component, and method to produce same.United States patent 8, 142, 892. 2012 Mar. 27.
10. Jeon, S. L., Chae, M. K., Jang, E. J. & Lee, C. Cleaved Iron Oxide Nanoparticles as T_2 Contrast Agents for Magnetic Resonance Imaging. *Chem. Eur. J.* **19**, 4217–4222 (2013).
11. Schneider, V. *et al.* Structural and Magnetic Properties of Ni/NiOxide - and Co/CoOxide Core/Shell Nanoparticles and their possible use for Ferrofluids. *Z. Phys. Chem.* **220**, 173–187 (2006).
12. Salazar-Alvarez, G., Sort, J., Suriñach, S., Baró, M. D. & Nogués, J. Synthesis and Size-Dependent Exchange Bias in Inverted Core−Shell MnO|Mn_3O_4 Nanoparticles. *J. Am. Chem. Soc.* **129**, 9102–9108 (2007).
13. Salazar-Alvarez, G. *et al.* Two-, Three-, and Four-Component Magnetic Multilayer Onion Nanoparticles Based on Iron Oxides and Manganese Oxides. *J. Am. Chem. Soc.* **133**, 16738–16741 (2011).
14. Krycka, K. L. *et al.* Correlating material-specific layers and magnetic distributions within onion-like Fe_3O_4/MnO/γ−Mn_2O_3 core/shell nanoparticles. *J. Appl. Phys.* **113**, 17B531 (2013).
15. Golosovsky, I. V. *et al.* Magnetic Proximity Effect Features in Antiferromagnetic/Ferrimagnetic Core–Shell Nanoparticles. *Phys. Rev. Lett.* **102**, 247201 (2009).
16. López-Ortega, A. *et al.* Size-Dependent Passivation Shell and Magnetic Properties in Antiferromagnetic/Ferrimagnetic Core/Shell MnO Nanoparticles. *J. Am. Chem. Soc.* **132**, 9398–9407 (2010).
17. Berkowitz, A. E. *et al.* Antiferromagnetic MnO nanoparticles with ferrimagnetic Mn_3O_4 shells: Doubly inverted core-shell system. *Phys. Rev. B* **77**, 024403 (2008).
18. Berkowitz, A. E. *et al.* Monodispersed MnO nanoparticles with epitaxial Mn_3O_4 shells. *J. Phys. D* **41**, 134007 (2008).
19. Kavich, D. W., Dickerson, J. H., Mahajan, S. V., Hasan, S. A. & Park, J. H. Exchange bias of singly inverted FeO/Fe_3O_4 core-shell nanocrystals. *Phys. Rev. B* **78**, 174414 (2008).
20. Chalasani, R. & Vasudevan, S. Form, Content, and Magnetism in Iron Oxide Nanocrystals. *J. Phys. Chem. C* **115**, 18088–18093 (2011).
21. Wetterskog, E., Tai, C. W., Grins, J., Bergström, L. & Salazar-Alvarez, G. Anomalous Magnetic Properties of Nanoparticles Arising from Defect Structures: Topotaxial Oxidation of $Fe_{1-x}O$|$Fe_{3-\delta}O_4$ Core|Shell Nanocubes to Single-Phase Particles. *ACS Nano* **7**, 7132–7144 (2013).
22. Khurshid, H. *et al.* Mechanism and controlled growth of shape and size variant core/shell FeO/Fe_3O_4 nanoparticles. *Nanoscale* **5**, 7942–7952 (2013).
23. Khurshid, H. *et al.* Synthesis and magnetic properties of core/shell FeO/Fe_3O_4 nanooctopods. *J. Appl. Phys.* **113**, 17B508 (2013).
24. Sun, X., Huls, N. F., Sigdel, A. & Sun, S. Tuning exchange bias in core/shell FeO/Fe_3O_4 nanoparticles. *Nano Lett.* **12**, 246–251 (2012).
25. Lak, A. *et al.* Size dependent structural and magnetic properties of FeO–Fe_3O_4 nanoparticles. *Nanoscale* **5**, 12286–12295 (2013).
26. Sharma, S. K. *et al.* Synthesis and ageing effect in FeO nanoparticles: Transformation to core–shell FeO/Fe_3O_4 and their magnetic characterization. *J. Alloy. Compd.* **509**, 6414–6417 (2011).
27. Bodnarchuk, M. I. *et al.* Exchange-Coupled Bimagnetic Wűstite/Metal Ferrite Core/Shell Nanocrystals: Size, Shape, and Compositional Control. *Small* **5**, 2247–2252 (2009).
28. Sytnyk, M. *et al.* Tuning the Magnetic Properties of Metal Oxide Nanocrystal Heterostructures by Cation Exchange. *Nano Lett.* **13**, 586–593 (2013).
29. Estarder, M. *et al.* Origin of the large dispersion of magnetic properties in nanostructured oxides: Fe_xO/Fe_3O_4 nanoparticles as a case study. *Nanoscale* **7**, 3002–3015 (2015).
30. Lima Jr., E. *et al.* Bimagnetic CoO Core/$CoFe_2O_4$ Shell Nanoparticles: Synthesis and Magnetic Properties. *Chem. Mater.* **24**, 512–516 (2012).
31. Winkler, E. L. *et al.* Origin of magnetic anisotropy in ZnO/$CoFe_2O_4$ and CoO/$CoFe_2O_4$ core/shell nanoparticle systems. *Appl. Phys. Lett.* **101**, 252405 (2012).
32. Lavorato, G. C. *et al.* Size effects in bimagnetic CoO/$CoFe_2O_4$ core/shell nanoparticles. *Nanotechnol.* **25**, 355704 (2014).
33. Baaziz, W. *et al.* Tuning of synthesis conditions by thermal decomposition towards core-shell $Co_xFe_{1-x}O@Co_yFe_{3-y}O_4$ and $CoFe_2O_4$ nanoparticles with spherical and cubic shapes. *Chem. Mater.* **26**, 5063–5073 (2014).
34. Fontaíña Troitiño, N., Rivas-Murias, B., Rodríguez-González, B. & Salgueiriño, V. Exchange Bias Effect in CoO@Fe_3O_4 Core−Shell Octahedron-Shaped. *Chem. Mater.* **26**, 5566–5575 (2014).
35. Liu, C., Cui, J., He, X. & Shi, H. Large exchange bias with remarkable thermostability in an inverted quasi core/shell CoO/γ-Fe_2O_3 granular system. *J. Nanopart. Res.* **16**, 2320 (2014)
36. Lavorato, G. C., Lima Jr., E.,Troiani, H. E., Zysler, R. D. & Winkler, E. L. Exchange-coupling in the termal annealed bimagnetic core/shell nanoparticles. *J. Alloy Compd.* **633**, 333–337 (2015).
37. Yun, B. K., Koo, Y. S. & Jung, J. H. Exchange Bias in Cr_2O_3/Fe_3O_4 Core/Shell Nanoparticles. *J. Magn.* **14**, 147–149 (2009).
38. Si, P. Z. *et al.* Synthesis, structure and exchange bias in $Cr_2O_3/CrO_2/Cr_2O_5$ particles. *Thin Solid Films* **519**, 8423–8425 (2011).
39. Jin, C. H. *et al.* Structure and magnetic properties of $Cr/Cr_2O_3/CrO_2$ microspheres prepared by spark erosion and oxidation under high pressure of oxygen. *Mater. Lett.* **92**, 213–215 (2013).
40. Basit, L. *et al.* Structure and magnetic properties of iron–platinum particles with γ-ferric-oxide shell. *Appl. Phys. A* **94**, 619–625 (2009).
41. Yusuf, S. M. *et al.* A study of exchange bias in $BiFeO_3$ core/$NiFe_2O_4$ shell nanoparticles. *J. Appl. Phys.* **113**, 173906 (2013).
42. Sung, K. D., Park, Y. A., Kim, K. Y., Hur, N. & Jung, J. H. Uncompensated spins in exchange-biased $BiFeO_3$/γ-Fe_2O_3 core/shell-like thin films. *J. Appl. Phys.* **114**, 103902 (2013).

43. Nogués, J., Skumryev, V., Sort, J. & Givord, D. Shell-Driven Magnetic Stability in Core-Shell Nanoparticles. *Phys. Rev. Lett.* **97**, 157203 (2006).
44. Margaris, G., Trohidou, K. N. & Nogués, J. Mesoscopic Model for the Simulation of Large Arrays of Bi-Magnetic Core/Shell Nanoparticles. *Adv. Mater.* **24**, 4331–4336 (2012).
45. Song, Q. & Zhang, Z. J. Controlled Synthesis and Magnetic Properties of Bimagnetic Spinel Ferrite $CoFe_2O_4$ and $MnFe_2O_4$ Nanocrystals with Core−Shell Architecture. *J. Am. Chem. Soc.* **134**, 10182–10190 (2012).
46. Estrader, M. *et al.* Robust antiferromagnetic coupling in hard-soft bi-magnetic core/shell nanoparticles. *Nat. Commun.* **4**, 2960 (2013).
47. Cai, J. W., Liu, K. & Chien, C. L. Exchange coupling in the paramagnetic state. *Phys. Rev. B* **60**, 72–75 (1999).
48. Sossmeier, K. D., Pereira, L. G., Schmidt, J. E. & Geshev, J. Exchange bias in a ferromagnet/antiferromagnet system with $T_C \ll T_N$. *J. Appl. Phys.* **109**, 083938 (2011).
49. Eftaxias, E. & Trohidou, K. N. Numerical study of the exchange bias effects in magnetic nanoparticles with core/shell morphology. *Phys. Rev. B* **71**, 134406 (2005).
50. Iglesias, O., Batlle, X. & Labarta, A. Microscopic origin of exchange bias in core/shell nanoparticles. *Phys. Rev. B* **72**, 212401 (2005).
51. Vasilakaki, M. & Trohidou, K. N. Numerical study of the exchange-bias effect in nanoparticles with ferromagnetic core/ferrimagnetic disordered shell morphology. *Phys. Rev. B* **79**, 144402 (2009).
52. López-Ortega, A. *et al.* Strongly exchange coupled inverse ferrimagnetic soft/hard, $MnxFe_{3-x}O_4/Fe_xMn_{3-x}O_4$, core/shell heterostructured nanoparticles. *Nanoscale* **4**, 5138–5147 (2012).
53. Vasilakaki, M., Eftaxias, E. & Trohidou, K. N. Monte Carlo study of the exchange bias and the training effect in nanoparticles with core/shell morphology. *Phys. Stat. Solid. A* **205**, 1865–1871 (2008).
54. Wu, M. H., Li, Q. C. & Liu, J. M. Monte Carlo simulation of size, random field and temperature dependences of exchange bias in a core/shell magnetic nanoparticle. *J. Phys.: Condens. Matter* **19**, 186202 (2007).
55. Hu, Y. & Du, A. Exchange bias in a nanogranular system with competing ferromagnetic and antiferromagnetic exchange interactions. *Phys. Stat. Solid. B* **248**, 2932–2940 (2011).
56. Hu, Y., Liu, Y., Qi, Y. & Du, A. Effect of Antiferromagnetic Anisotropy on Exchange Bias in a Single Composite Nanoparticle with Unconventional Antiferromagnetic-Ferromagnetic Core-Shell Morphology. *e-J Surf. Sci. Nanotech.* **9**, 67–71 (2011).
57. Néel, L. Théorie du paramagnétisme constant; application au manganese. *C. R. Acad. Sc.* **203**, 304–306 (1936).
58. Sort, J. *et al.* Coercivity and squareness enhancement in ball-milled hard magnetic–antiferromagnetic composites. *Appl. Phys. Lett.* **79**, 1142–1144 (2001).
59. Sort, J. *et al.* Improving the energy product of hard magnetic materials. *Phys. Rev. B* **65**, 174420 (2002).
60. Bødker, F., Mørup, S., & Linderoth, S. Surface Effects in Metallic Iron Nanoparticles. *Phys. Rev. Lett.* **72**, 282–285 (1994).
61. Dimitrov, D. A. & Wysin, G. M. Magnetic properties of superparamagnetic particles by a Monte Carlo method. *Phys. Rev. B* **54**, 9237–9241 (1996).
62. Bottcher, D., Ernest, A. & Henk, J. Temperature-dependent Heisenberg exchange coupling constants from linking electronic-structure calculations and Monte Carlo simulations. *J. Magn. Magn. Mater.* **324**, 610–615 (2012).
63. Estradé, S. *et al.* Distinguishing the core from the shell in MnO_x/MnO_y and FeO_x/MnO_x core/Shell nanoparticles through quantitative electron energy loss spectroscopy (EELS) analysis. *Micron* **43**, 30–36 (2012).
64. Binder, K. & Heermann, D. W. *Applications of Monte Carlo Methods in Statistical Physics* (Springer-Verlag 1984).

Acknowledgments

M.V. and K.N.T. acknowledge the financial support of the European Social Fund (EU) and the Greek National Operational Program "Education and Lifelong Learning" in the framework of ARISTEIA I (Project COMANA/22). J.N. acknowledges the support of the 2014-SGR-1015 project of the Generalitat de Catalunya and the MAT2010-20616-C02 and MAT2013-48628-R projects of the Spanish Ministerio de Econimía y Competitibidad (MINECO). Part of the calculations used resources of the Hellas Grid computing infrastructure. ICN2 acknowledges support from the Severo Ochoa Program (MINECO, Grant SEV-2013-0295).

Author contributions

K.N.T. and J.N. designed the experiments. M.V. and K.N.T. performed the simulations. K.N.T. and J.N. wrote the manuscript. All authors contributed to the analysis and discussion.

Additional information

Competing financial interests: The authors declare no competing financial interests.

How to cite this article: Vasilakaki, M., Trohidou, K.N. & Nogués, J. Enhanced Magnetic Properties in Antiferromagnetic-Core/Ferrimagnetic-Shell Nanoparticles. *Sci. Rep.* **5**, 9609; DOI:10.1038/srep09609 (2015).